

# Toluene Processed All-Polymer Solar Cells with 18% Efficiency and Enhanced Stability Enabled by Solid Additive: Comparison between Sequential-Processing and Blend-Casting

Guoping Zhang<sup>1</sup>, Chaoyue Zhao<sup>1</sup>, Liangxiang Zhu<sup>1</sup>, Lihong Wang<sup>1</sup>, Wenzhao Xiong<sup>2</sup>, Huawei Hu<sup>2</sup>, Qing Bai<sup>1</sup>, Yaping Wang<sup>1</sup>, Chen Xie<sup>1</sup>, Peng You<sup>1</sup>, He Yan<sup>3</sup>, Dan Wu<sup>1</sup>, Tao Yang<sup>1</sup>, Mingxia Qiu<sup>1</sup>, Shunpu Li<sup>1</sup>, and Guangye Zhang<sup>1</sup>

<sup>1</sup>Shenzhen Technology University

<sup>2</sup>Donghua University

<sup>3</sup>The Hong Kong University of Science and Technology

August 7, 2023

## Abstract

The emergence of polymerized small molecule acceptors (PSMAs) has significantly improved the performance of all-polymer solar cells (all-PSCs). However, the pace of device engineering lacks behind that of materials development, so that a majority of the PSMAs have not fulfilled their potentials. Furthermore, most high-performance all-PSCs rely on the use of chloroform as the processing solvent. For instance, the recent high-performance PSMA named PJ1- $\gamma$ , with high LUMO and HOMO levels, could only achieve a PCE of 16.1% with a high-energy-level donor (JD40) using chloroform. Herein, we present a methodology combining sequential processing (SqP) with the addition of 0.5%wt PC71BM as a solid additive (SA) to achieve an impressive efficiency of 18.0% for all-PSCs processed from toluene, an aromatic hydrocarbon solvent. Compared to the conventional blend-casting (BC) method whose best efficiency (16.7%) could only be achieved using chloroform, the SqP method significantly boosted the device efficiency using toluene as the processing solvent. In addition, the donor we employ is the classic PM6 that has deeper energy levels than JD40, which provides low energy loss for the device. We compare the results with another PSMA (PYF-T-o) with the same method. Finally, an improved photostability of the SqP devices with the incorporation of SA is demonstrated.

## Toluene Processed All-Polymer Solar Cells with 18% Efficiency and Enhanced Stability Enabled by Solid Additive: Comparison between Sequential-Processing and Blend-Casting

Guoping Zhang,<sup>a+</sup> Chaoyue Zhao,<sup>ad+</sup> Liangxiang Zhu,<sup>a+</sup> Lihong Wang<sup>a</sup>, Wenzhao Xiong<sup>c</sup>, Huawei Hu<sup>c</sup>, Qing Bai<sup>a</sup>, Yaping Wang<sup>a</sup>, Chen Xie<sup>a</sup>, Peng You<sup>a</sup>, He Yan<sup>d</sup>, Dan Wu,<sup>a\*</sup> Tao Yang,<sup>b\*</sup> Mingxia Qiu,<sup>a\*</sup> Shunpu Li,<sup>a\*</sup> Guangye Zhang<sup>a\*</sup>

<sup>a</sup> College of New Materials and New Energies, Shenzhen Technology University, Shenzhen 518118, China

Email: wudan@sztu.edu.cn; qiumingxia@sztu.edu.cn; lishunpu@sztu.edu.cn; zhangguangye@sztu.edu.cn

<sup>b</sup> Julong College, Shenzhen Technology University, Shenzhen 518118, China

Email: yangtao@sztu.edu.cn

<sup>c</sup> State Key Laboratory for Modification of Chemical Fibers and Polymer Materials, Center for Advanced Low-dimension Materials, College of Materials Science and Engineering, Donghua University, Shanghai, 201620 China

<sup>d</sup> Department of Chemistry and Hong Kong Branch of Chinese National Engineering Research Center for Tissue Restoration and Reconstruction, The Hong Kong University of Science and Technology, Clear Water Bay, Hong Kong, 999077 China

<sup>+</sup> These authors contributed equally to this work

## Abstract

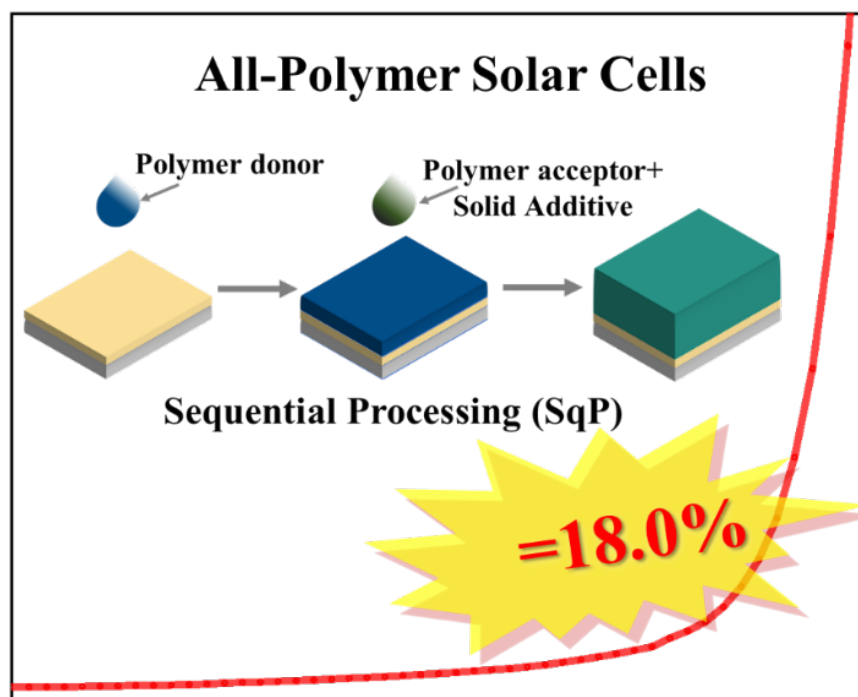
The emergence of polymerized small molecule acceptors (PSMAs) has significantly improved the performance of all-polymer solar cells (all-PSCs). However, the pace of device engineering lags behind that of materials development, so that a majority of the PSMAs have not fulfilled their potentials. Furthermore, most high-performance all-PSCs rely on the use of chloroform as the processing solvent. For instance, the recent high-performance PSMA named PJ1- $\gamma$ , with high LUMO and HOMO levels, could only achieve a PCE of 16.1% with a high-energy-level donor (JD40) using chloroform. Herein, we present a methodology combining sequential processing (SqP) with the addition of 0.5%wt PC<sub>71</sub>BM as a solid additive (SA) to achieve an impressive efficiency of 18.0% for all-PSCs processed from toluene, an aromatic hydrocarbon solvent. Compared to the conventional blend-casting (BC) method whose best efficiency (16.7%) could only be achieved using chloroform, the SqP method significantly boosted the device efficiency using toluene as the processing solvent. In addition, the donor we employ is the classic PM6 that has deeper energy levels than JD40, which provides low energy loss for the device. We compare the results with another PSMA (PYF-T-*o*) with the same method. Finally, an improved photostability of the SqP devices with the incorporation of SA is demonstrated.

**Key words:** all-polymers solar cells, sequential processing, solid additive

## Highlight

The lack of device engineering limits the performance of many promising polymer acceptors. We employ a combined effort of the sequential processing technique and the incorporation of solid additive to significantly promote the all-polymer solar cell device (18%) with the polymerized small molecule acceptor (PJ1r). The device is made from toluene instead of the commonly used chloroform. An enhanced photostability is observed in the 18% device.

## TOC



## Introduction

All-polymer solar cells (all-PSCs) hold great promise for future advancements in the field of organic solar cells thanks to their excellent film-formation and excellent properties.<sup>[1-11]</sup> To date, the highest PCE achieved in all-PSCs has surpassed 18%<sup>[12-14]</sup> thanks to the rapid development of polymer acceptors, especially the recent strategy of polymerizing high-performance small molecule acceptors.<sup>[15-25]</sup> Nevertheless, the development of these polymerized small molecule acceptors (PSMAs) is so rapid that there is a gap between the exhibited performance and the highest achievable performance of the materials due to the relatively slow pace of device engineering. For instance, Yang et al. recently reported a PSMA named PJ1r, whose frontier orbital energy levels are uplifted compared to the popular PSMA such as PY-IT and PYF-T-o, which should promote the voltage of the device in principle. However, the best PCE reported so far of this PSMA was only about 16.1%,<sup>[26]</sup> achieved using a polymer donor (JD40) with an uplifted LUMO and HOMO levels than the workhorse donor, PM6. This could benefit exciton dissociation but it undermined the potential of the PSMA to achieve high Voc.

Furthermore, the best efficiency of most recent high-performance all-PSCs was achieved using chloroform as the processing solvent including PJ1r.<sup>[12-13, 27-37]</sup> In addition to its hazardous properties, chloroform has a high vapor pressure at temperatures relevant to device fabrication, making it unsuitable for large-scale fabrication techniques such as slot-die coating and blade-coating.<sup>[38-46]</sup> To take advantage of the superior film-formation properties and mechanical properties of all-PSCs in future large-scale productions, chloroform must be replaced processing solvent with a high boiling point at standard pressure, preferentially non-halogen solvents.

In this paper, we combined the sequential processing (SqP) technique and a solid additive strategy to address the aforementioned issues, namely, promoting the performance of existing PSMAs and using hydrocarbon solvent to replace chloroform. Compared to the conventional blend-casting (BC) method that relies on their inherent crystallization kinetics to achieve vertical phase separation, the SqP technique separates the preparation of the donor and acceptor solutions and the deposition of them, which utilizes the mutual solubility of the upper solution with the underlying film to form a bicontinuous interpenetrating network

structure known as the bulk heterojunction (BHJ). On the basis of SqP, we further mix a tiny amount of PC<sub>71</sub>BM into the active layer as a solid additive (SA) to tune the morphology and electrical properties of all-PSCs in this study. Specifically, we first employ PM6 as the donor polymer and PJ1- $\gamma$  as the acceptor to fabricate binary all-PSC devices. We demonstrate a 17.4% PCE for the SqP PM6:PJ1-r device compared to a 15.8% PCE for the BC device. Subsequently, when 0.5% PC<sub>71</sub>BM is introduced as a solid additive into the active layer, the PCE is further increased to 18.0%. Film-depth-dependent light absorption spectra (FLAS) reveals that the addition of the SA improves the vertical phase segregation of the active layer, leading to enhanced charge carrier lifetime, reduced carrier extraction time, increased electron mobility, and more balanced electron/hole transport, which in turn contributes to the high photocurrent. Moreover, we carry out the same experiments using another PSMA (PYF-T-*o*) and provide side-by-side comparison between the devices with these two acceptors. We show that the addition of the SA also increases the performance of the PYF-T-*o* devices. Finally, the maximum power point tracking (MPPT) technique is used to study the device stability. We show that both the incorporation of SA and the SqP method improve the photo-stability of the device.

## Results and Discussion

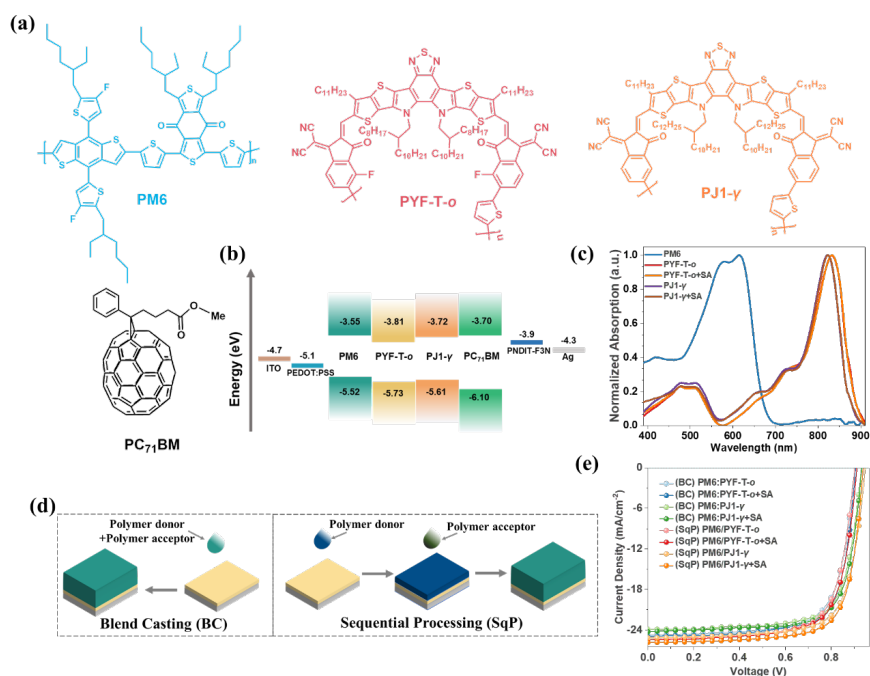


**Figure 1.** (a) Chemical structures of PM6, PYF-T-*o*, PJ1- $\gamma$  and PC<sub>71</sub>BM; (b) energy level diagram; (c) UV-Vis absorption spectra of pure PM6, pure acceptor and acceptor:SA (1000:5 weight ratio) films; (d) Schematic diagram showing the difference between blend-casting and sequential processing; (e) Current density-voltage ( $J$ - $V$ ) curves.

**Figure 1a** depicts the molecular structures of poly(benzodithiophene-4,8-dione) (PM6), PYF-T-*o*, PJ1- $\gamma$ , and [6,6]-phenyl-C<sub>71</sub>-butyric acid methyl ester (PC<sub>71</sub>BM). **Figure 2b** illustrates the energy levels of the active layer materials,<sup>[26, 47-48]</sup> where PJ1- $\gamma$  exhibits higher LUMO (-3.72 eV) and HOMO levels (-5.61 eV) than PYF-T-*o*. Therefore, the PJ1- $\gamma$  based solar cell has a greater potential to realize a high  $V_{oc}$  upon similar energy losses. **Figure 1c** presents the UV-vis absorption spectra of the pure films of the donor and acceptors as well as those of the polymer acceptor:SA films. The main absorption of PM6 ranges from 500 nm to 650 nm, while the acceptors exhibit strong absorption in the range of 750 nm to 850 nm. The absorption profiles of the donor and acceptor complement each other, allowing for the absorption of a broader

range of photons. Furthermore, the introduction of the tiny amount of PC<sub>71</sub>BM into the active layer does not alter the optical density (in the resolution relevant for OSC devices), which suggests that the role of PC<sub>71</sub>BM in promoting device performance should mainly be its contribution in morphology and electrical properties. The UV-Vis absorption spectra of the blend films are shown in the Supporting Information (SI, **Figure S1**), which shows a similar donor-to-acceptor ratio between the different films. This is advantageous in minimizing the influence of the donor-to-acceptor ratio on device performance when comparing different device engineering techniques.

Conventional devices with a structure of ITO/PEDOT:PSS/active layer/PDNIT-F3N/Ag were fabricated, where the active layer was prepared using either the BC or the SqP method (see **Figure 1d**). To investigate the effect of solvents on device performance, the BC device was fabricated from either chloroform or toluene. More detailed device preparation procedure is available in the **SI**. The device configurations using the BC method were denoted as (BC)PM6:PYF-T-*o*, (BC)PM6:PYF-T-*o* +SA (with the addition of SA), (BC)PM6:PJ1- $\gamma$ , and (BC)PM6:PJ1- $\gamma$  +SA. The corresponding SqP devices were denoted by (SqP)PM6/PYF-T-*o*, (SqP)PM6/PYF-T-*o* +SA, (SqP)PM6/PJ1- $\gamma$ , and (SqP)PM6/PJ1- $\gamma$  +SA. **Figure 1e** shows the *J-V* curves of the devices obtained from the measurements, and the detailed photovoltaic parameters are summarized in **Table 1**, **Table S2** and **Table S3**. When toluene (Tol) was used as the processing solvent, the maximum power conversion efficiencies (PCEs) of the (BC)PM6:PJ1- $\gamma$  (Tol) and (BC)PM6:PJ1- $\gamma$  +SA(Tol) devices are 15.8% and 16.2%, respectively. The best performance for BC devices can only be achieved using chloroform (CF) as the processing solvent: The (BC)PM6:PJ1- $\gamma$  and (BC)PM6:PJ1- $\gamma$  +SA show maximum PCEs of 16.5% and 16.7%, respectively. As we mentioned above, we also prepared PYF-T-*o* and PJ1- $\gamma$  devices using the SqP method where the processing solvent for both the donor and acceptor materials was toluene. First, in the binary device, the SqP method improved the efficiency of PJ1- $\gamma$ -based device by 1.6%, resulting in a PCE of 17.4% for the binary device of (SqP)PM6/PJ1- $\gamma$ , with a  $V_{OC}$  of 0.947 V, a  $J_{SC}$  of 25.18 mA cm<sup>-2</sup>, and a FF of 0.731. Next, the addition of the small amount of solid additive successfully boosted the PCE of the toluene-processed SqP device, (SqP)PM6/PJ1- $\gamma$  +SA, to 18.0%, which is among the highest PCEs for all-polymer solar cells processed from non-halogen solvent. The improvement by the SA was also observed in the PYF-T-*o* based all-PSC devices.

**Table 1.** Summary of photovoltaic parameters for PM6, PYF-T-*o*, PJ1- $\gamma$  based all-PSCs processed from different methods, measured under AM 1.5 G illumination at 100 mW cm<sup>-2</sup>.

Active layer	$V_{OC}$ [V]	$J_{SC}$ [mA/cm <sup>2</sup> ]	$J_{EQE}$ [mA/cm <sup>2</sup> ]	$J_{EQE}$ [mA/cm <sup>2</sup> ]	FF[%]	PCE <sup>(a)</sup> [%]
(BC) PM6:PYF-T- <i>o</i>	0.902(0.900±0.002)	24.9(24.7±0.4)	24.9(24.7±0.4)	24.5	71.6(70.5±0.9)	16.1(15.7±0.2)
(BC) PM6:PYF-T- <i>o</i> +SA	0.906(0.904±0.002)	24.9(24.7±0.4)	24.9(24.7±0.4)	24.7	74.7(73.6±1.2)	16.9(16.5±0.2)
(BC) PM6:PJ1- $\gamma$	0.932(0.932±0.002)	24.0(23.7±0.4)	24.0(23.7±0.4)	23.7	73.8(73.6±1.4)	16.5(16.2±0.2)
(BC) PM6:PJ1- $\gamma$ +SA	0.933(0.934±0.002)	24.2(24.0±0.4)	24.2(24.0±0.4)	24.1	73.9(73.2±0.6)	16.7(16.4±0.2)
(BC) PM6:PJ1- $\gamma$ (Tol)	0.938(0.940±0.002)	23.8(23.4±0.7)	23.8(23.4±0.7)	23.3	70.9(70.22±1.5)	15.8(15.4±0.3)
(BC) PM6:PJ1- $\gamma$ +SA(Tol)	0.942(0.941±0.001)	24.0(23.6±0.4)	24.0(23.6±0.4)	23.5	71.6(71.9±0.8)	16.2(16.0±0.1)

Active layer	$V_{OC}$ [V]	$J_{SC}$ [mA/cm <sup>2</sup> ]	$J_{EQE}$ [mA/cm <sup>2</sup> ]	$J_{EQE}$ [mA/cm <sup>2</sup> ]	FF[%]	PCE <sup>(a)</sup> [%]
(SqP) PM6/PYF-T- <i>o</i>	0.901(0.906±0.005)	23.4(25.1±0.4)	25.4(25.1±0.4)	24.6	71.4(71.0±1.0)	16.4(16.1±0.2) 16.4(16.1±0.2)
(SqP) PM6/PYF-T- <i>o</i> +SA	0.910(0.908±0.002)	23.5(25.1±0.2)	25.5(25.1±0.2)	25.1	72.4(72.7±0.6)	16.8(16.6±0.1) 16.8(16.6±0.1)
(SqP) PM6/PJ1- $\gamma$	0.947(0.943±0.004)	23.2(25.0±0.3)	25.2(25.0±0.3)	24.6	73.1(73.1±0.8)	17.4(17.3±0.1) 17.4(17.3±0.1)
(SqP) PM6/PJ1- $\gamma$ +SA	0.937(0.938±0.001)	23.9(25.7±0.2)	25.9(25.7±0.2)	25.0	74.3(74.3±0.4)	18.0(17.9±0.1) 18.0(17.9±0.1)

<sup>(a)</sup> The standard deviations are based on measurements of over at least ten independent devices.

As shown in **Figure 2a** and **2b**, when the SqP method is used, the devices exhibit higher external quantum efficiencies (EQEs) in the 600-800 nm range compared to the BC devices. As a result, the EQE integrated current density of the devices increased from 23.7 mA/cm<sup>2</sup> to 25.0 mA/cm<sup>2</sup> when the SqP method was employed in the PJ1- $\gamma$  system. From the perspective of additives, the addition of the SA also contributes to a general improvement in efficiency compared to the SA-free binary devices. As shown in **Table 1**, the greatest improvement in device performance is about 0.8% between the (BC) PM6/PYF-T-*o* +SA and (BC) PM6/PYF-T-*o* devices. Such improvement by the applying of SA is also demonstrated in (SqP)PM6/PJ1- $\gamma$  +SA, (BC)PM6:PJ1- $\gamma$  +SA devices and (SqP)PM6/PYF-T-*o* +SA devices, compared to their corresponding devices without the SA.

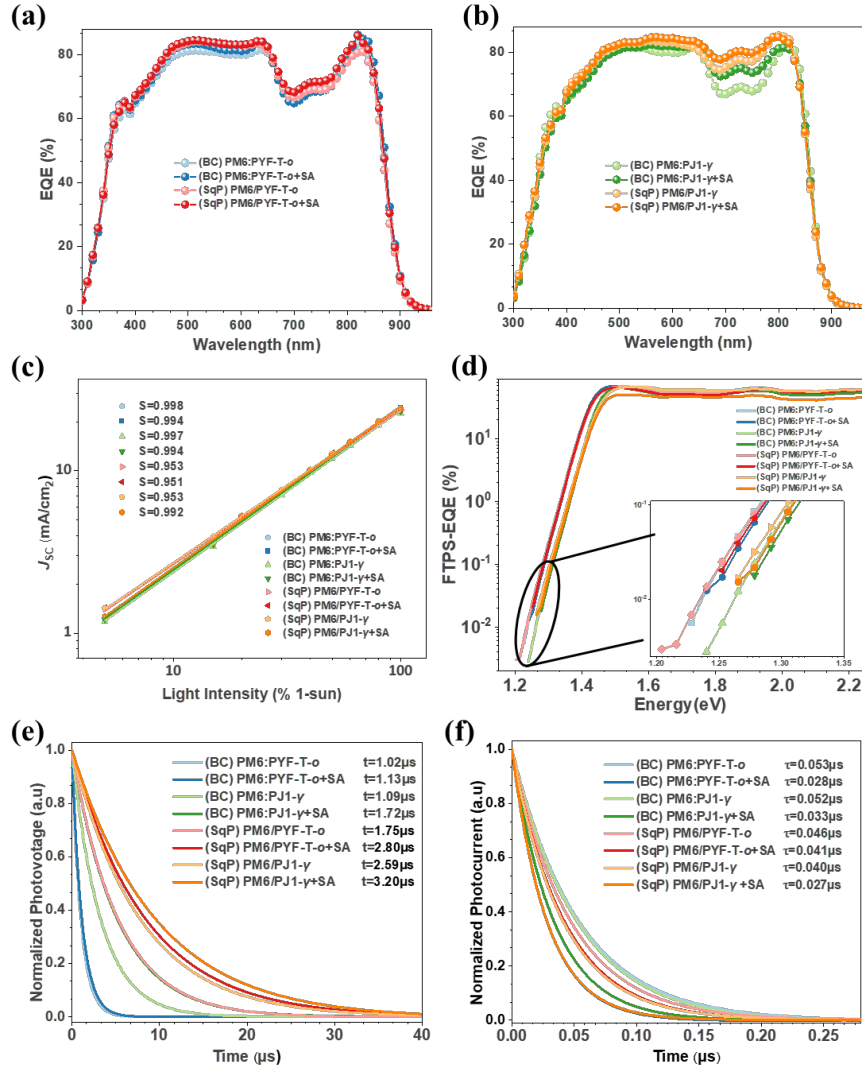


**Figure 2.** (a) External quantum efficiency (EQE) spectra for PM6 and PYF-T-*o* based all-PSC devices; (b) EQE spectra for PM6 and PJ1- $\gamma$  based devices; (c)  $J_{SC}$  versus light intensity of different devices; (d) FTPS-EQE spectra measured from 500 to 1800 nm; inset: a zoom-in view of the EQE spectra in the low energy region; (e) TPV decay curves for devices; (f) TPC decay curves for devices.

The incorporation of SA, along with the utilization of the SqP method, effectively improves the device performance, particularly in the PJ1- $\gamma$  system. To understand the charge carrier transport and recombination, we first measured the variation of  $J_{SC}$  relative to light intensity (plotted on a logarithmic scale) in **Figure 2c**, where the slope  $S$  of each data set is fitted and listed. Typically,  $S$  falls within the range of 0.8-1.0, and the variation in the numerical value of  $S$  within this range is mainly attributed to the loss of charge carriers in bimolecular recombination. Overall, BC devices have slightly less bimolecular recombination than SqP devices, but the difference is small, and the best device in SqP has bimolecular recombination similar to that in BC devices. For BC devices, the  $S$  value for (BC)PM6:PYF-T-*o* is 0.998, for (BC)PM6:PYF-T-*o*+SA is 0.994, for (BC)PM6:PJ1- $\gamma$  is 0.997, and for (BC)PM6:PJ1- $\gamma$ +SA is 0.994. For SqP devices, the  $S$  value for (SqP)PM6/PYF-T-*o* is 0.953, for (SqP)PM6/PYF-T-*o*+SA is 0.951, for PM6/PJ1- $\gamma$  is 0.953, and for PM6/PJ1- $\gamma$ +SA is 0.992. We also investigated the variation of  $V_{OC}$  under different light intensities, and

the results, reflected by the ideality factor,  $n_{id,1}$  (**Figure S2**), showed two trends: Firstly, the SqP method significantly reduces the trap-assisted recombination as the  $n_{id,1}$  values are much lower than those of the BC devices; Secondly, the addition of the SA further decreases the trap-assisted recombination in the SqP devices, but not so strongly as it does in the BC devices. To summarize the combined effects of SqP and SA: SqP does not show improvements in bimolecular recombination without the aid of SA, but significantly reduces trap-assisted recombination, which is further reduced when SA is incorporated.

High-sensitivity EQE measurements were employed to investigate trap states in this study: Sub-bandgap EQE was measured via Fourier-transformed photocurrent spectroscopy (FTPS), and the resulting photocurrent spectra for the BC devices and SqP devices are presented in **Figure 2d**. Due to noise, the low-energy signals were truncated. The inset of **Figure 2d** displays a clear quantum efficiency for all devices in the low-energy region (e.g.,  $\sim 1.20$ - $1.28$  eV), which is likely attributed to the presence of deep trap states within the bandgap, resulting in relatively poor FF values for the devices. Notably, devices prepared via the SqP method exhibited fewer states in the low-energy region overall compared to those prepared using the BC method. The trend observed for the devices in the low-energy region of the FTPS test aligns with that of the  $n_{id}$  values. In order to gain insights into charge recombination and extraction, transient photovoltage (TPV) and transient photocurrent (TPC) experiments were conducted, the results of which are shown in **Figure 2e** and **2f**, respectively. Compared to devices prepared using the BC method, devices prepared using the SqP method display a slower TPV decay and a faster TPC decay. The decay constants are obtained by fitting the TPV and TPC decay curves with a single exponential function. For BC devices, the TPV decay constants and TPC decay constants are  $1.02\mu\text{s}$ ,  $1.13\mu\text{s}$ ,  $1.09\mu\text{s}$ , and  $1.72\mu\text{s}$ , and  $0.053\mu\text{s}$ ,  $0.028\mu\text{s}$ ,  $0.052\mu\text{s}$ , and  $0.033\mu\text{s}$  for (BC)PM6:PYF-T-*o*, (BC)PM6:PYF-T-*o* +SA, (BC)PM6:PJ1- $\gamma$ , and (BC)PM6:PJ1- $\gamma$  +SA. For SqP devices, the TPV decay constants and TPC decay constants are  $1.75\mu\text{s}$ ,  $2.80\mu\text{s}$ ,  $2.59\mu\text{s}$ , and  $3.20\mu\text{s}$ , and  $0.046\mu\text{s}$ ,  $0.041\mu\text{s}$ ,  $0.040\mu\text{s}$ , and  $0.027\mu\text{s}$  for (SqP)PM6/PYF-T-*o*, (SqP)PM6/PYF-T-*o* +SA, (SqP)PM6/PJ1- $\gamma$ , and (SqP)PM6/PJ1- $\gamma$  +SA. We note that the TPV decay constant is referred to as the carrier “lifetime” in some literature, but it has been shown that the constant is affected by charge carrier mobilities and interfacial properties of the device in the TPV measurement, so we choose to stay with the term “TPV decay constant” in this work, which could have contributions from the bulk lifetime and can only be used as an indication of it. Overall, the TPV and TPC results seems to suggest that both the SqP method and the incorporation of the SA may make the charge carriers live longer and be extracted easier compared to the BC method or the SA-free devices.

To assess the charge carrier transport property, we employed the space-charge limited current (SCLC) model to calculate the electron and hole mobilities. The details of SCLC device fabrication and data analysis can be found in the experimental section of the Supplementary Information and in **Figure S3**, and the calculated mobilities are summarized in **Table S3**. As we have demonstrated in our previous reports,<sup>[47, 49]</sup> due to the low degree of polymerization of the PSMA compared to the high degree of polymerization of the donor polymers such as PM6, and their relatively weaker crystallization/aggregation tendency compared to small molecule acceptors, the electron mobility in the recent PSMA-based all-PSC device is generally lower than the hole mobility in the same BC device. For instance, the electron mobility of the (BC)PM6:PYF-T-*o* device is  $2.40 \times 10^{-4} \text{ cm}^2 \text{ V}^{-1} \text{ s}^{-1}$  while the hole mobility is  $4.14 \times 10^{-4} \text{ cm}^2 \text{ V}^{-1} \text{ s}^{-1}$ . From the SCLC results in **Table S3**, we found that the electron mobility can be improved by both the SqP method and the incorporation of the SA, particularly in the PYF-T-*o*-based devices. The enhanced electron mobility is crucial for the devices with a conventional architecture where more excitons are generated in the bottom part (near the anode) that we will discuss in details later.

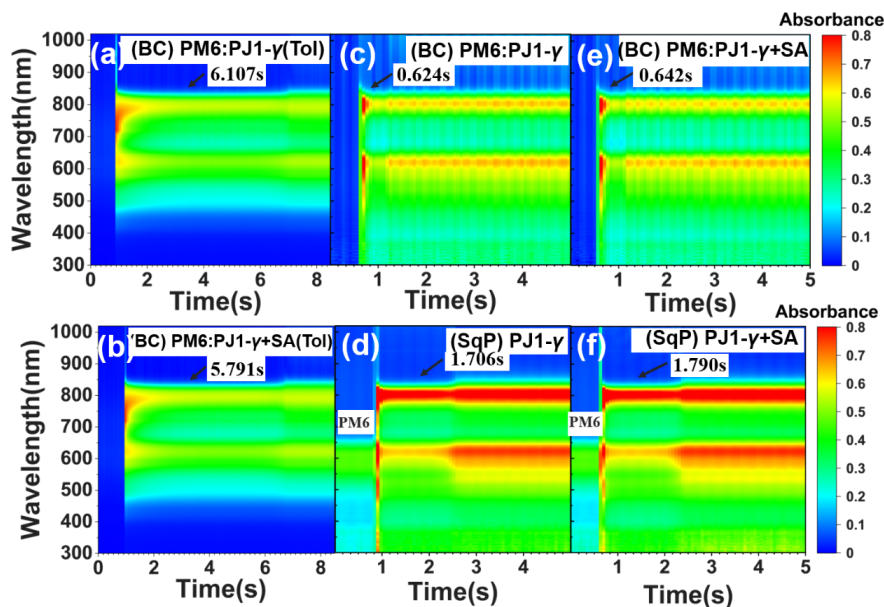


**Figure 3.** In situ UV-Vis absorption spectra to show the formation of active layer using the the BC (a-c, e) and SqP (d, f).

To further evaluate the film formation process in the active layer, we conducted in-situ UV measurements, which monitors the variation of the absorption spectra during the active layer film-formation process. The change in raw optical density with respect to deposition time is shown in **Figure S4**. **Figure 3** is the mapping of the evolution of absorbance at each wavelength for the BC and SqP films during their liquid-to-solid transitions. First, in the BC method, the film-formation time (from the deposition of the blend solution to the time when the UV-vis density stops changing) for the toluene (Tol) solution ( $>5$  s) is much longer than the chloroform solution ( $<0.7$ s), as expected. The addition of the SA in the BC method causes an increase in the film-formation time when the solvent is chloroform but a decrease in the toluene-based solution. In the SqP method, the deposition of the acceptor solution make the donor's absorption resemble that of the liquid state, suggesting a high degree of swelling. Then, the donor and acceptor precipitates during the evaporation of toluene, and the drying times for the without and with SA solution are 1.706 and 1.790, respectively. The time for the acceptor being co-dissolved with the donor in the solution is obviously much shorter than the BC method, which has a higher possibility to make the domain of the acceptor or donor purer by reducing the intermixing time. It is worth noting that in the best-performing BC (with chloroform) and SqP (with toluene) systems, the addition of the solid additive increases the film formation time, by 18 ms for the PJ1- $\gamma$  system for the BC film and by 84 ms for the SqP film.

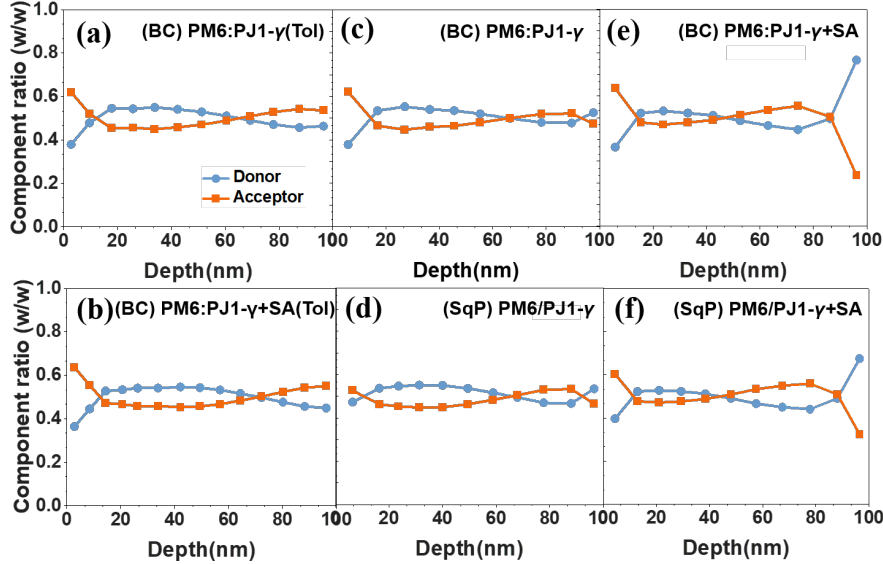


**Figure 4.** Composition ratio across the vertical direction of the active layer film by FLAS base on BC film (a-c,e) and SqP film (d,f).

Next, we investigate the effect of SqP and SA on the vertical phase segregation of the active layer. To this end, film-depth-dependent light absorption spectra (FLAS) were measured on the BC and SqP films. By sequentially etching the film using plasma while monitoring the changes in absorption spectra in real-time (etching spectra shown in **Figure S5**), the vertical distribution profile (**Figure 4**), exciton generation profile in the vertical direction (**Figure S6**), and exciton generation rate curve in the vertical direction (**Figure S7**) were calculated using the transfer matrix model.<sup>[50-51]</sup> The vertical distribution profiles (**Figure 4a-f**) show distinct differences in the final distribution due to the variations in film preparation methods as well as in material structures of the acceptors. In the PJ1- $\gamma$  system, the introduction of the solid additive does not alter the vertical phase segregation in the BC films prepared with toluene, but it results in noticeable adjustments to the vertical morphology for BC films processed from chloroform and the SqP films from toluene: The addition of the SA make the bottom portion of the active layer (closer to the anode) exhibit a higher concentration of donor and a lower concentration of acceptor than those without the SA, which is beneficial for interfacial charge selectivity. The trends in the vertical phase segregation for these films are well consistent with the trend in their device electrical properties such as the TPV and TPC decay constants and fill factor. Similar observation has been made in the PYF-T-*o*-based system (**Figure S9**) with an additional effect provided by the SA: the incorporation of the SA leads to a more uniform distribution of donor and acceptor in the middle region of the active layer.

To evaluate the miscibility between the materials from a thermodynamics point of view, surface tensions of the materials are first analyzed. The contact angle of different solvents on the solid films are shown in **Figure S8**. We calculated the surface tension ( $\gamma$ ) of each material or material combination based on Wu’s model and the interfacial tension between materials as an indication of miscibility. Generally, a lower interfacial tension value indicates a higher miscibility between the materials at thermal equilibrium. As presented in **Table S5**, the interfacial tension value between PM6 and PYF-T-*o* is 0.03 mN/m, while that between PM6 and PJ1- $\gamma$  is 0.67 mN/m. In comparison, the miscibility between PJ1- $\gamma$  and PM6 is weaker, particularly when the solid additive is introduced (the interfacial tension increases to 2.08 mN/m). This suggests that compared to PM6:PYF-T-*o*, PJ1- $\gamma$  has a higher tendency to phase separate from the donor during the film formation. Furthermore, the fact that the SqP reduces the intermixing time indicates that the SqP method could regulate the degree of phase separation to some extent.

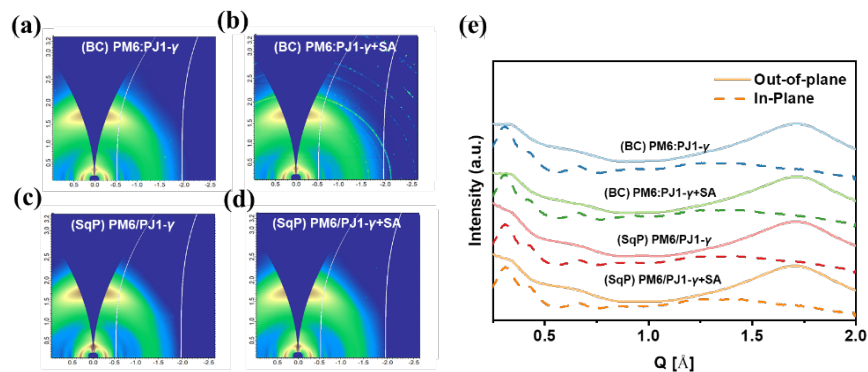


**Figure 5.** (a-d) The 2D-GIWAXS patterns of blend films base on PJ1- $\gamma$ . (e) The in-plane and out-of-plane line cuts of the 2D GIWAXS patterns for the blend films base on PJ1- $\gamma$ .

To examine the molecular stacking and crystallinity of different films, grazing-incidence wide-angle X-Ray scattering (GIWAXS) experiments were conducted. **Figures 5a-5d** displays the two-dimensional patterns and line-cuts along the out-of-plane and in-plane directions of the blended films prepared from either SqP or BC method. The  $d$ -spacing and crystal coherence length (CCL) of these films are summarized in **Table S6**. The  $\pi$ - $\pi$  stacking distances for all four films were found to be 3.70 Å. The CCL values for (BC)PM6:PJ1- $\gamma$ , (BC)PM6:PJ1- $\gamma$ +SA, (SqP)PM6/PJ1- $\gamma$ , and (SqP)PM6/PJ1- $\gamma$ +SA are 16.8 Å, 16.9 Å, 16.7 Å, and 16.2 Å, respectively. Notably, the  $d$ -spacing and CCL between the PYF-T- $o$  and PJ1- $\gamma$  films are largely different (**Table S1**). For example, the CCLs for the (100) peak of the PYF-T- $o$  base blend films are in the range of 54-58 Å, while those of the PJ1- $\gamma$  based films are in the range of 88-95 Å, highlighting the effect of the difference in the miscibility between materials on the phase separation behavior of the blend film.

**Figure 6.** Normalized PCE change with light-soaking time using an MPP tracking method for the BC and SqP devices.

The long-term photostability of all-PSC is crucial for their future commercial application. To assess the photostability of different all-PSCs, we continuously monitored the performance of the optimized (BC)PM6:PJ1- $\gamma$  and (BC)PM6:PJ1- $\gamma$ +SA devices and their SqP counterparts under 1 sun LED illumination in a test chamber. As shown in **Figure 6**, the (BC)PM6:PJ1- $\gamma$  device has a rapid decrease in PCE with a T80 value of  $\sim$ 65 h. In contrast, the SqP method and the addition of SA both lead to enhanced stability than the BC device. Specifically, after adding SA, the T80 value of the (BC)PM6:PJ1- $\gamma$ +SA device slightly increases from about 65 h device to 140 h. Furthermore, the SA-free SqP device shows a significant increase in T80 value to nearly 250 h. Notably, after over 300 h of continuous illumination, the (SqP)PM6/PJ1- $\gamma$ +SA devices exhibit the highest photostability (T80 value is almost 310 h). The result that the SqP method could increase T80 of all-PSC has been reported in our previous reports using other material combinations, which is further confirmed by this work. The surprising result of this work is that the incorporation of the small amount of SA further promotes the stability of the all-PSCs.

## Conclusion

In conclusion, the incorporation of a small amount of solid additive into the binary all-polymer system has successfully achieved a maximum PCE of 18% in devices sequentially processed from the hydrocarbon solvent, toluene, which is among the highest PCEs of non-halogen solvent processed all-PSCs. This demonstrates a relatively simple approach to further enhance the performance of all-PSCs. We studied four different comparisons side-by-side in this work, namely, toluene vs. chloroform, blend-casting vs. sequential processing, SA-free vs SA, PYF-T- $o$ vs PJ1- $\gamma$ . Finally, the stability of the devices was assessed using MPPT, and the SqP devices with SA exhibited approximately 80% PCE retention after continuous exposure to 1-sun illumination for over 400 hours. This presents a new avenue for exploring highly efficient and stable

all-polymer systems in future research.

## Supporting Information

Supplementary data associated with this article can be found in the online version at XXX

## Acknowledgement

G. Z., C. Z., and L. Z. contributed equally to this work. The work was supported by the Guangdong Basic and Applied Basic Research Foundation (2022A1515010875), Guangdong Basic and Applied Basic Research Foundation (2021A1515110017), Natural Science Foundation of Top Talent of SZTU (grant no. 20200205), Project of Education Commission of Guangdong Province of China (2021KQNCX080), Research on the electrochemical reaction mechanism of the anode of medium-Low temperature direct ammonia SOFCs (20231063020006), the project of all solid-state high energy density energy storage system (20221063010031) and the project of Shenzhen Overseas Talent upon Industrialization of 1kw stack for direct ammonia SOFCs (20221061010002). S. L. would like to thank Guangdong Basic and Applied Basic Research Foundation (No. 2019A1515011673), Education Department of Guangdong Province (No. 2021KCXTD045) and National Natural Science Foundation of China (No. 12274303). H. H. thanks for the support from the Fundamental Research Funds for the Central Universities (2232023A-01), NSFC No. 52103202 and beamline BL16B1 at Shanghai Synchrotron Radiation Facility (SSRF) for the synchrotron experiment.

## Author Contribution

Guoping Zhang: Investigation, conceptualization, writing-original, writing-review & editing, performing experiments and analysis Chaoyue Zhao: Analysis about GIWAXS and devices fabrication, writing-review & editing Liangxiang Zhu: Device fabrication, J-V measurements, Contact angle test and formal analysis Lihong Wang: Data analysis on device J-V characteristics and light intensity dependence studies Wenzhao Xiong: GIWAXS experiments and data analysis Huawei Hu: GIWAXS experiments and data analysis, and providing resources for morphology investigation Qing Bai: Investigation and formal analysis Yaping Wang: Participated in device testing and formal analysis Chen Xie: Investigation on properties of active layer and formal analysis Peng You: Investigation on properties of active layer and formal analysis He Yan: Resources on materials Dan Wu: Analysis of the EQE & UV-Vis absorption results Tao Yang: Analysis of the AFM and mobility results Mingxia Qiu: Resources on J-V characterization, EQE, and supervision Shunpu Li: Resources on device fabrication, J-V measurements, supervision, and funding acquisition Guangye Zhang: Resources on laboratory, supervision of the whole project, funding acquisition that supported most of the project, project administration, writing manuscript, revision & editing

## Reference

- [1] K. K. Zhou, K. H. Xian, Q. C. Qi, M. Y. Gao, Z. X. Peng, J. W. Liu, Y. Liu, S. M. Li, Y. D. Zhang, Y. H. Geng, L. Ye, *Advanced Functional Materials* **2022** , 32, 14.
- [2] Y. Zhang, B. Q. Wu, Y. K. He, W. Y. Deng, J. W. Li, J. Y. Li, N. Qiao, Y. F. Xing, X. Y. Yuan, N. Li, C. J. Brabec, H. B. Wu, G. H. Lu, C. H. Duan, F. Huang, Y. Cao, *Nano Energy* **2022** , 93, 11.
- [3] G. Zeng, W. J. Chen, X. B. Chen, Y. Hu, Y. Chen, B. Zhang, H. Y. Chen, W. W. Sun, Y. X. Shen, Y. W. Li, F. Yan, Y. F. Li, *J. Am. Chem. Soc.* **2022** , 144, 8658.
- [4] Y. C. Liang, D. F. Zhang, Z. R. Wu, T. Jia, L. Luer, H. R. Tang, L. Hong, J. B. Zhang, K. Zhang, C. J. Brabec, N. Li, F. Huang, *Nat. Energy* **2022** , 7, 1180.
- [5] Z. G. Zhang, Y. F. Li, *Angew. Chem.-Int. Edit.* **2021** , 60, 4422.
- [6] R. Sun, W. Wang, H. Yu, Z. Chen, X. X. Xia, H. Shen, J. Guo, M. M. Shi, Y. N. Zheng, Y. Wu, W. Y. Yang, T. Wang, Q. Wu, Y. Yang, X. H. Lu, J. L. Xia, C. J. Brabec, H. Yan, Y. F. Li, J. Min, *Joule* **2021** , 5, 1548.
- [7] B. Kan, F. Ershad, Z. Y. Rao, C. J. Yu, *Nano Research* **2021** , 14, 2891.

- [8] Y. Song, K. Zhang, S. Dong, R. X. Xia, F. Huang, Y. Cao, *ACS Appl. Mater. Interfaces* **2020** , 12, 18473.
- [9] G. Zeng, W. Chen, X. Chen, Y. Hu, Y. Chen, B. Zhang, H. Chen, W. Sun, Y. Shen, Y. Li, F. Yan, Y. Li, *J. Am. Chem. Soc.* **2022** , 144, 8658.
- [10] Y. Song, K. Zhang, S. Dong, R. Xia, F. Huang, Y. Cao, *ACS Appl. Mater. Interfaces* **2020** , 12, 18473.
- [11] Y. W. Han, S. J. Jeon, H. S. Lee, H. Park, K. S. Kim, H.-W. Lee, D. K. Moon, *Advanced Energy Materials* **2019** , 9, 1902065.
- [12] R. Sun, T. Wang, Q. Fan, M. Wu, X. Yang, X. Wu, Y. Yu, X. Xia, F. Cui, J. Wan, X. Lu, X. Hao, A. K. Y. Jen, E. Spiecker, J. Min, *Joule* **2023** , 7, 221.
- [13] R. Ma, Q. Fan, T. A. Dela Peña, B. Wu, H. Liu, Q. Wu, Q. Wei, J. Wu, X. Lu, M. Li, W. Ma, G. Li, *Advanced Materials* **2023** , 35, 2212275.
- [14] Y. Cai, C. Xie, Q. Li, C. Liu, J. Gao, M. H. Jee, J. Qiao, Y. Li, J. Song, X. Hao, H. Y. Woo, Z. Tang, Y. Zhou, C. Zhang, H. Huang, Y. Sun, *Advanced Materials* **2023** , 35, 2208165.
- [15] J. Wang, Y. Cui, Y. Xu, K. Xian, P. Bi, Z. Chen, K. Zhou, L. Ma, T. Zhang, Y. Yang, Y. Zu, H. Yao, X. Hao, L. Ye, J. Hou, *Advanced Materials* **2022** , 34, 2205009.
- [16] Y. Li, Q. Li, Y. H. Cai, H. Jin, J. Q. Zhang, Z. Tang, C. F. Zhang, Z. X. Wei, Y. M. Sun, *Energy & Environmental Science* **2022** , 15, 3854.
- [17] C. Zhang, Z. W. Ge, J. W. Xue, W. Ma, Y. M. Sun, *Macromolecular Chemistry and Physics* **2023** , 224, 7.
- [18] B. Q. Wu, Y. L. Li, S. Z. Tian, Y. Zhang, L. H. Pan, K. Z. Liu, M. Q. Yang, F. Huang, Y. Cao, C. H. Duan, *Chinese Journal of Chemistry* **2023** , 41, 790.
- [19] P. Wang, Y. H. Zhu, H. X. Tao, Y. L. Ma, D. D. Cai, Q. S. Tu, R. C. Liao, Q. D. Zheng, *Chinese Journal of Polymer Science* **2023** , DOI: 10.1007/s10118-023-2909-39.
- [20] C. Wang, C. Guan, T. Wu, X. Q. Liu, J. Fang, F. Liu, C. Y. Xiao, W. W. Li, *ACS Appl. Mater. Interfaces* **2023** , 15, 13363.
- [21] Z. Q. Zhang, D. Deng, Y. Li, J. W. Ding, Q. Wu, L. L. Zhang, G. J. Zhang, M. J. Iqbal, R. Wang, J. Q. Zhang, X. H. Qiu, Z. X. Wei, *Advanced Energy Materials* **2022** , 12, 10.
- [22] Z. Y. Li, F. Peng, H. L. Quan, X. T. Qian, L. Ying, Y. Cao, *Chem. Eng. J.* **2022** , 430, 9.
- [23] Y. X. Kong, Y. X. Li, J. Y. Yuan, L. M. Ding, *Infomat* **2022** , 4, 8.
- [24] T. Jia, J. B. Zhang, H. R. Tang, J. C. Jia, K. Zhang, W. Y. Deng, S. Dong, F. Huang, *Chem. Eng. J.* **2022** , 433, 8.
- [25] K. Hu, J. Q. Du, C. Zhu, W. B. Lai, J. Li, J. M. Xin, W. Ma, Z. J. Zhang, J. Y. Zhang, L. Meng, Y. F. Li, *Sci. China-Chem.* **2022** , 65, 954.
- [26] J. C. Jia, Q. R. Huang, T. Jia, K. Zhang, J. Zhang, J. S. Miao, F. Huang, C. L. Yang, *Advanced Energy Materials* **2022** , 12, 9.
- [27] Q. Ma, Z. R. Jia, L. Meng, H. Yang, J. Y. Zhang, W. B. Lai, J. Guo, X. Jiang, C. H. Cui, Y. F. Li, *Advanced Functional Materials* **2023** , 33, 8.
- [28] L. Zhang, T. Jia, L. Pan, B. Wu, Z. Wang, K. Gao, F. Liu, C. Duan, F. Huang, Y. Cao, *Science China Chemistry* **2021** , 64, 408.
- [29] H. Sun, B. Liu, Y. Ma, J.-W. Lee, J. Yang, J. Wang, Y. Li, B. Li, K. Feng, Y. Shi, B. Zhang, D. Han, H. Meng, L. Niu, B. J. Kim, Q. Zheng, X. Guo, *Advanced Materials* **2021** , 33, 2102635.

- [30] T. Jia, J. Zhang, W. Zhong, Y. Liang, K. Zhang, S. Dong, L. Ying, F. Liu, X. Wang, F. Huang, Y. Cao, *Nano Energy* **2020** , 72, 104718.
- [31] K. Feng, Z. Wu, M. Su, S. Ma, Y. Shi, K. Yang, Y. Wang, Y. Zhang, W. Sun, X. Cheng, L. Huang, J. Min, H. Y. Woo, X. Guo, *Advanced Functional Materials* **2021** , 31, 2008494.
- [32] C. Duan, Z. Li, S. Pang, Y.-L. Zhu, B. Lin, F. J. M. Colberts, P. J. Leenaers, E. Wang, Z.-Y. Sun, W. Ma, S. C. J. Meskers, R. A. J. Janssen, *Solar RRL* **2018** , 2, 1800247.
- [33] C. Shang, S. Zhang, D. Han, X. Ding, Y. Zhang, C. Yang, J. Ding, X. Bao, *ACS Appl. Mater. Interfaces* **2023** , 15, 5538.
- [34] G. P. Zhang, L. H. Wang, C. Y. Zhao, Y. J. Wang, R. Y. Hu, J. X. Che, S. Y. He, W. Chen, L. F. Cao, Z. H. Luo, M. X. Qiu, S. P. Li, G. Y. Zhang, *Polymers* **2022** , 14, 11.
- [35] Y. Yue, B. Zheng, J. Ni, W. Yang, L. Huo, J. Wang, L. Jiang, *Advanced Science* **2022** , 9, 2204030.
- [36] B. Li, X. Zhang, Z. Wu, J. Yang, B. Liu, Q. Liao, J. Wang, K. Feng, R. Chen, H. Y. Woo, F. Ye, L. Niu, X. Guo, H. Sun, *Science China Chemistry* **2022** , 65, 1157.
- [37] K. An, F. Peng, W. Zhong, W. Deng, D. Zhang, L. Ying, H. Wu, F. Huang, Y. Cao, *Science China Chemistry* **2021** , 64, 2010.
- [38] J. Y. Zhang, L. F. Zhang, X. K. Wang, Z. J. Xie, L. Hu, H. D. Mao, G. D. Xu, L. C. Tan, Y. W. Chen, *Advanced Energy Materials* **2022** , 12, 8.
- [39] J. X. Li, X. C. Meng, Z. Q. Huang, R. Y. Dai, W. P. Sheng, C. X. Gong, L. C. Tan, Y. W. Chen, *Advanced Functional Materials* **2022** , 32, 10.
- [40] D. Chen, S. Q. Liu, B. Huang, J. Oh, F. Y. Wu, J. B. Liu, C. Yang, L. Chen, Y. W. Chen, *Small* **2022** , 18, 9.
- [41] Z. Xing, X. C. Meng, R. Sun, T. Hu, Z. Q. Huang, J. Min, X. T. Hu, Y. W. Chen, *Advanced Functional Materials* **2020** , 30, 7.
- [42] S. Q. Liu, D. Chen, X. T. Hu, Z. Xing, J. Wan, L. Zhang, L. C. Tan, W. H. Zhou, Y. W. Chen, *Advanced Functional Materials* **2020** , 30, 8.
- [43] Z. Q. Huang, X. T. Hu, Z. Xing, X. C. Meng, X. P. Duan, J. Long, T. Hu, L. C. Tan, Y. W. Chen, *J. Phys. Chem. C* **2020** , 124, 8129.
- [44] X. C. Meng, L. Zhang, Y. P. Xie, X. T. Hu, Z. Xing, Z. Q. Huang, C. Liu, L. C. Tan, W. H. Zhou, Y. M. Sun, W. Ma, Y. W. Chen, *Advanced Materials* **2019** , 31, 10.
- [45] X. C. Meng, X. T. Hu, X. Yang, J. P. Yin, Q. X. Wang, L. Q. Huang, Z. K. N. Yu, T. Hu, L. C. Tan, W. H. Zhou, Y. W. Chen, *ACS Appl. Mater. Interfaces* **2018** , 10, 8917.
- [46] X. T. Hu, X. C. Meng, J. Xiong, Z. Q. Huang, X. Yang, L. C. Tan, Y. W. Chen, *Adv. Mater. Technol.* **2017** , 2, 8.
- [47] C. Zhao, J. Yi, L. Wang, G. Lu, H. Huang, H. K. Kim, H. Yu, C. Xie, P. You, G. Lu, M. Qiu, H. Yan, S. Li, G. Zhang, *Nano Energy* **2022** , 104, 107872.
- [48] N. Al-Shekaili, S. Hashim, F. F. Muhammadsharif, M. Z. Al-Abri, K. Sulaiman, M. Y. Yahya, M. Ridzuan Ahmed, *Materials Today: Proceedings* **2021** , 42, 1921.
- [49] C. Zhao, R. Ma, Y. Hou, L. Zhu, X. Zou, W. Xiong, H. Hu, L. Wang, H. Yu, Y. Wang, G. Zhang, J. Yi, L. Chen, D. Wu, T. Yang, G. Li, M. Qiu, H. Yan, S. Li, G. Zhang, *Advanced Energy Materials* **2023** , DOI: 10.1002/aenm.202300904.

[50] Y. Zhang, D. Deng, Z. Wang, Y. Wang, J. Zhang, J. Fang, Y. Yang, G. Lu, W. Ma, Z. Wei, *Advanced Energy Materials***2017** , 7, 1701548.

[51] L. Bu, S. Gao, W. Wang, L. Zhou, S. Feng, X. Chen, D. Yu, S. Li, G. Lu, *Advanced Electronic Materials***2016** , 2, 1600359.